An Analytical Model for Pitch Moment Stiffness of Bolted Connections and Its Application in Ballscrew Bearing Support Block Selection

Akshay D. Harlalka¹

Department of Mechanical Engineering, Massachusetts Institute of Technology, 77 Massachusetts Ave, Cambridge, MA 02139 e-mail: akshayh@alum.mit.edu

Alexander H. Slocum

Department of Mechanical Engineering, Massachusetts Institute of Technology, 77 Massachusetts Ave, Cambridge, MA 02139 e-mail: slocum@mit.edu Bolted joints are commonly used structural connections as they provide a strong secure joint along with ease of assembly/disassembly. While analytical models for the axial stiffness of bolted joints are well developed, models for moment (angular) stiffness of bolted structures, such as ball screw bearing support blocks, are needed to help engineers rapidly design more efficient precision machines. This paper develops a parametric moment stiffness model for bolted connections which is verified via numerical and experimental methods. Application of the model is illustrated with a ball screw system design spreadsheet, available in Supplemental Material on the ASME Digital Collection, applied to two case studies (machine tool linear axis and high-speed 3D printer) to show how predicting the moment stiffness of ball screw support bearing blocks helps in expanding the available design space and enhance the design performance. [DOI: 10.1115/1.4054474]

Keywords: ballscrews, bolted connections, moment stiffness, pillow blocks, bolted joints, design of machine elements, design theory

1 Introduction

The computation of bolted connection stiffness has been studied since the early 1970s with a focus on stiffness in axial and lateral directions [1-6]. The stiffness ratio between the bolt and the clamped members directly governs the fraction of the load that will be safely carried by the bolt [3]. Zhang and Poirier [1] presented a model for bolted joints that considers effects related to rotation of the members and their additional deformation when subjected to external loads and verified the model with finite element analysis (FEA). Nassar and Abboud [2] proposed an improved stiffness model based on more accurate determination of the effective joint area where the strain cone angle was experimentally determined and various effects related to joint sizes, under head contact radii ratio, and plate material/thickness ratio were investigated. The results of the proposed model agreed well with experimental data and FEA. Other studies have focused on the computation of member stiffness. Lehnhoff et al. [4] calculated the member stiffness of various bolted connections (with different bolt sizes, materials, and thicknesses). Dimensionless curves were presented in the paper to help the audience estimate the member stiffness ratios for a variety of bolted joints. The analytical predictions were in moderate agreement with FEA. Sethuraman and Sasi Kumar [5] did a similar evaluation of member stiffness of axisymmetric bolted connections and proposed various empirical formulas for computation of the same which were in agreement with the FEA. The study of pressure distribution among bolted members has also been motivated by interests in other domains of electric or thermal power across bolted connections. Gould and Mikic [7] studied the pressure distribution in the contact zones and

determined the radii of separation of the bolted members using experimental and finite element methods which were also in agreement with FEA. Studies have found that in all cases, variables such as clamping pressure distribution [8], and the changing contact condition of the members under external loads [9], contribute to the stiffness of bolted connections.

These theories, however, do not directly apply to the moment stiffness of bolted joint connections and FEA and experiments are generally too costly. So engineers often use rules-of-thumb or copy what has been done before which may not lead to good results. In a fast-paced engineering environment, analytical models are needed for rapidly creating and developing viable design concepts. Once a design has been selected and developed in this manner, FEA can then be economically used to check the design and ensure an adequate safety factor.

The moment stiffness of bolted connections is an important design parameter for engineers working on the design of precision machines. One such example is a design of ball screw drive system. The selection of a ball screw drive system for a given application is often an iterative process as shown in ball screw supplier catalogs [10]. Knowledge of the system stiffness helps develop servo control models and predict positioning accuracy. The system stiffness is a function of the stiffness of the screw shaft, nut, support bearings, and housing which are strongly affected by bolted joint stiffness. Established guidelines are available to predict the stiffness of all these components except the moment stiffness of the housing. The theory presented in this paper can be used to predict the stiffness of bearing block housing thereby helping the designer to determine the full stiffness model as a part of the ball screw selection procedure.

An analytical model is presented herein for the moment stiffness of a bolted connection and is verified via finite element analysis and experimental testing. Three different ball bearing mounting blocks (i.e., pillow blocks) are used as examples. For each pillow block,

¹Corresponding author.

Manuscript received November 13, 2021; final manuscript received April 25, 2022; published online July 19, 2022. Assoc. Editor: Joshua Summers.

analytical calculations, FEA solutions, and experimental testing results are compared and discussed.

Herein, Secs. 2–4 develop the stiffness analysis of bolted pillow blocks and discuss the generic FEA analysis procedure, and detail the experimental setup. Sections 5–10 present the results of the study for three types of pillow blocks. Opportunities for further work observed during this study are presented in the Conclusion.

2 Development of Analytical Model for Pitch Moment Stiffness of Bolted Connections

2.1 Sources of Compliance. Consider a steel pillow block bolted onto an aluminum base (Fig. 1) and a model of the stiffness along the pillow block axis (Fig. 2). Consider the base to be fixed, there are two main sources of compliance in the system: one related to the compliance of the pillow block itself (shear, bending, and torsion) and the other related to the bolted joint stiffness. Since the focus of this paper is on prediction of the joint stiffness, a pillow block with much greater inherent stiffness than its bolted connection was preferred for study, so the system stiffness will be dominated by joint stiffness.

2.2 Different Cases. To investigate the efficacy of the analytical model, pitch moment stiffnesses ("pitch stiffness") of three different types of pillow blocks were assessed with the model and compared with the experimental data and numerical solution. The pillow blocks include 2-bolt type with steel body, 4-bolt type with steel body, and 2-bolt type with plastic polylactic acid (PLA) body (Fig. 3). For experimental measurements, the predicted pitch stiffness is transformed into a linear transverse stiffness parallel to the direction of pillow block axis. While the load is applied along the axis of the pillow block and the deflection is measured at the tip of the block as shown in Fig. 1. This is also useful to the machine designer when considering the stiffness of a mounted ball screw for example.

2.3 Nomenclature. Table 1 represents various symbols used in the development of the analytical model and how they relate to the bolted pillow block assembly (Fig. 1).

2.4 Joint Stiffness: Pitch

2.4.1 Axial Joint Stiffness Model. The axial stiffness of the joint is governed by the stiffness of different members in the structural loop, including the bolt stiffness and the member stiffness. The traditional spring model of the bolted joint and a visualization of the

strain cone with a half-apex angle of α is represented in Figs. 4(a) and 4(b), respectively. The shape of the pressure distribution among the clamped members of a bolted connection is complex, and Shigley [11] suggests the use of simpler cone geometry with a half-apex angle of 30 deg to approximate the shape of the strain cone. For members with unequal thickness and materials, the calculation of the member stiffness becomes cumbersome. As per Shigley [11] and Williams [12], for the case of members with unequal thicknesses, the strain cone extends up to half of the effective grip length (p) of the clamped members and then begins to recede for the other half of the grip length. Generally, it is desirable to make the strain cones of the bolted connections overlap in order to prevent inducing any straightness errors on the parts being bolted [13].

This theory can be visualized with photoelastic experiments of plexiglass members of unequal thicknesses. To observe the stress field, the bolted assembly was kept directly in front of a polarized light source (a liquid crystal display (LCD) screen in this case). A circular polarizer filter (55 mm diameter) was rotated accordingly to block the light from the LCD screen and to observe the stress fields from the plexiglass members clearly. Figures 5(a) and 5(b) show these stress fields in the clamped members. Stress birefringence is just one of the many methods to observe strain cones and contact pressure distribution in interfaces. Researchers have also used ultrasonic measurements [14] and pressure film sensors [15] to investigate the distribution of contact pressure and predict interfacial contact stiffnesses.

a. Member stiffness calculation:

Traditional model

From Fig. 4(b), it can be seen that the flange consists of two frustums and the bed consists of a single frustum. To compute the member stiffness of the flange, the compliances of the two frustums need to be calculated separately and then added together using Eq. (8). As per Shigley [11], Eq. (1) can be used to calculate the compliance of a frustum under the head of the bolt.

$$C_{\text{top|frustum}} = \frac{\ln \left[\frac{(2h_1 \tan \alpha + D - d)(D + d)}{(2h_1 \tan \alpha + D + d)(D - d)} \right]}{\pi E_{\text{flange}} d \tan \alpha}$$
(1)

It can be observed from Eq. (1) that the compliance of the frustum depends on its height, half-apex angle of the cone, bolt major and head diameters, and the elastic modulus of the material. The height of top and bottom frustums of the flange $(h_1 \text{ and } h_2)$ can be derived using simple geometry from Fig. 4(b) (refer Eqs. (3) and (4)). A cone angle of 30 deg is used for the calculation. The

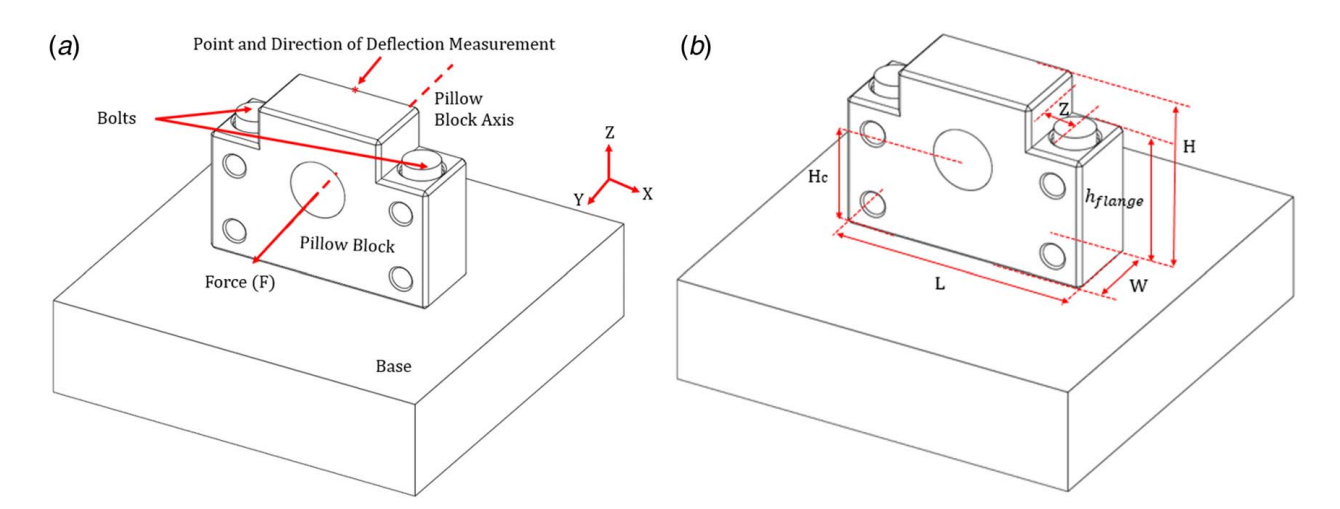


Fig. 1 Illustrations of a pillow block assembly mounted on a metal base: (a) pillow block assembly and (b) dimensional representations

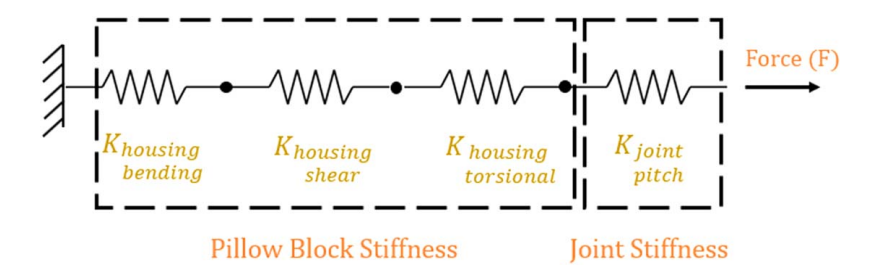


Fig. 2 Spring model of the pillow block mounted on a metal base



Fig. 3 Different test cases: (a) 2-bolt pillow block (steel), (b) 4-bolt pillow block (steel), and (c) 2-bolt pillow block (PLA)

flange (pillow block) is made of plain carbon steel ($E_{\rm flange}$ = 200 GPa). The total effective grip length includes the height of the flange and the height of the base material in grip. Since, this is a tapped joint, the equivalent height of the base material in grip can be assumed to be equal to half the bolt diameter [11]. For the

Table 1 Symbols used in the development of analytical model

Symbol	Meaning			
W	Width of the pillow block			
Н	Total height of the pillow block			
H_c	Height of the pillow block axis			
H_t	Depth at which threads start in the base			
L [.]	Length of the pillow block			
E	Young's modulus			
$E_{\rm flange}$	Young's modulus of pillow block (flange)			
E_{bed}	Young's modulus of base (bed)			
I	Moment of inertia			
G	Shear modulus			
θ	Angle of twist			
J	Polar moment of inertia			
h_1	Height of the top cone frustum of flange			
h_2	Height of the bottom cone frustum of flange			
$h_{ m bg}$	Height of base material in grip			
h_{flange}	Height of the pillow block (flange) at bolt underside			
h_{bed}	Height of the bed			
t	Effective thickness for shear stiffness calculation			
d	Bolt major diameter			
D	Bolt head diameter			
D'	Interfacial contact diameter			
α	Half-apex angle of the cone			
p	Effective grip length of the clamped members			
A_d	Area of unthreaded portion of bolt			
A_t	Area of threaded portion of bolt			
l_d	Length of unthreaded portion of bolt in grip			
l_t	Length of threaded portion of bolt in grip			
τ	Shear stress			
F	Force			
C_x	Compliance of <i>x</i>			
K_x	Stiffness of x			
$Z^{"}$	Length of the side flange of pillow block measured from bolt			
	centerline to main body			
$P_{\rm ext}$	Pressure due to external loading			
$P_{ m preload}$	Preload pressure			

detailed overview of the bolt parameters and the calculations, please see Supplemental Material on the ASME Digital Collection.

$$p = h_{\text{flange}} + h_{\text{bg}} \tag{2}$$

$$h_1 = p/2 = (h_{\text{flange}} + h_{\text{bg}})/2$$
 (3)

$$h_2 = p/2 - h_{\rm bg} \tag{4}$$

$$h_{\rm bg} = d/2 \tag{5}$$

Equation (1) only considers the stiffness of the top frustum. A similar equation can be used to compute the stiffness of the bottom frustum (Eq. (6)). However, to do so, two parameters will need to be modified. The head diameter (D) will need to be replaced by the interfacial contact diameter (D') and the thickness of the cone frustum will need to be h_2 . The interfacial contact diameter can be calculated using simple geometry as per Eq. (7).

$$C_{\rm bottom|frustum} = \frac{\ln \left[\frac{(2h_2 \tan \alpha + D' - d)(D' + d)}{(2h_2 \tan \alpha + D' + d)(D' - d)} \right]}{\pi E_{\rm flange} d \tan \alpha} \tag{6}$$

$$D' = D + 2h_{\rm bg} \tan \alpha \tag{7}$$

To find the equivalent flange compliance, the compliances of the top and bottom frustum are added in Eq. (8). For bed compliance calculation (Eq. (9)), the height of the frustum is same as the height of the base material in grip. The equivalent head diameter (D) for the bed cone frustum can be assumed to be 1.5d [11], which is almost equal to the bolt head diameter (D).

$$C_{\text{flange}|\text{comp}} = C_{\text{top}|\text{frustum}} + C_{\text{bottom}|\text{frustum}}$$
 (8)

$$C_{\rm bed|comp} = \frac{\ln \left[\frac{(2h_{\rm bg} \tan \alpha + D - d)(D + d)}{(2h_{\rm bg} \tan \alpha + D + d)(D - d)} \right]}{\pi E_{\rm bed} d \tan \alpha} \tag{9}$$

In the traditional member stiffness model represented by Fig. 4(a), the equivalent member stiffness of a bolted connection

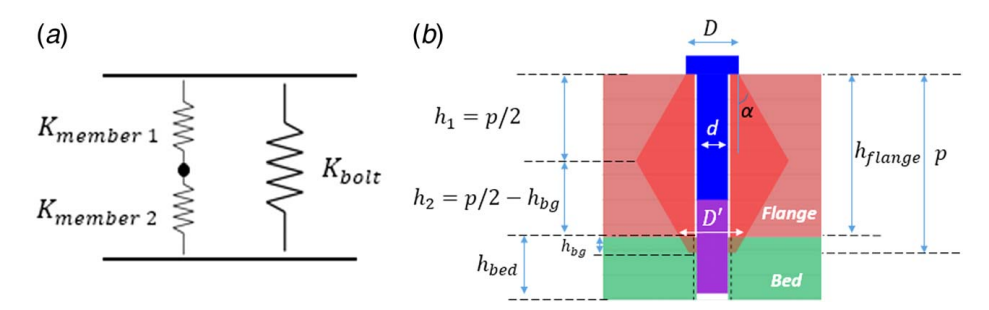


Fig. 4 Bolted connection visualization and spring model: (a) conventional spring model of the axial joint stiffness and (b) bolt visualization

can be calculated using Eq. (10).

$$K_{\text{member(Traditional)}} = \frac{1}{C_{\text{flange|comp}} + C_{\text{bed|comp}}}$$
 (10)

Contribution of shear stiffness

While some bolted connection spring models [11] take just compression stiffness of the members into consideration, other spring models take the member shear stiffness also into account [13]. Hence experimental data on member stiffness from earlier literature were gathered and compared to results from FEA simulations and various hypothesized analytical models. Some of these analytical models took shear stiffness into account while other models did not. An FEA model corresponding to a member stiffness experiment setup from the published literature [16] was created and its results were compared with published experimental data for validation. After validation, FEA results were used to pick the accurate analytical model for member stiffness.

Analytical, FEA, and experimental validation of member stiffness

a. Experimental results

Maruyama [16] used a simple experimental setup to determine the axial stiffness of the members in a bolted connection. The setup consisted of a circular plate with a hole and two pressure pieces, simulating bolt head, and nut to apply the axial load. The diameter of the hole was 25 mm and the diameter of the circular plate was 100 mm. The material of the circular plate was S45C (designated according to the Japanese Steel Grading System). Its American equivalent is AISI 1045. A single circular plate was used as a replacement for two clamped members found in a bolted

connection. The experimental value for stiffness of this member was reported to be 565 kgf/um or 5540 N/um [16].

b. FEA results

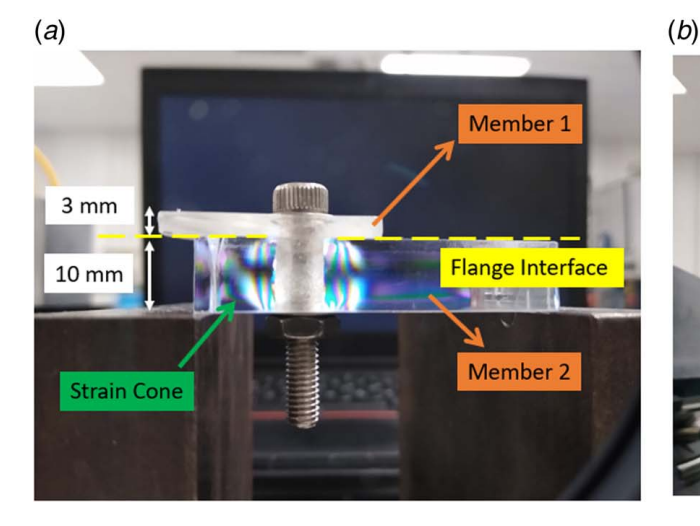
Using the same geometry of the circular plate and pressure plates used in Maruyama's experimental setup, the deformation of the member plate was simulated with FEA. As the objective of the model was to probe the member stiffness only, the bolt shank, head, and nut were not modeled. The faces of the circular plate at the interface locations of the pressure plate were subdivided. All degrees-of-freedom at the bottom pressure plate interface were fixed, while for the top pressure plate interface, only X and Ydegrees-of-freedom were fixed. The X-Y constraint on the top interface was important because the model assumed no occurrence of slip between the circular member plate and the pressure plates. Based on the FEA result, the stiffness of the clamped plate was reported to be 5555 N/um, which is very close to Maruyama's experimental result of 5540 N/um. For a visual representation of the loads and constraints applied during this analysis, please refer to Fig. 7(a).

c. Analytical results

Using the member compliance formulas (Eqs. (1)–(10)) listed by Shigley [11], a theoretical prediction of the member stiffness can be made. For the parameters corresponding to Maruyama's experimental setup, the axial stiffness of the member plate is calculated to be 6420 N/um.

d. Conclusion

Based on the aforementioned values, the FEA, experimental, and theoretical calculations are in reasonable agreement with each other.



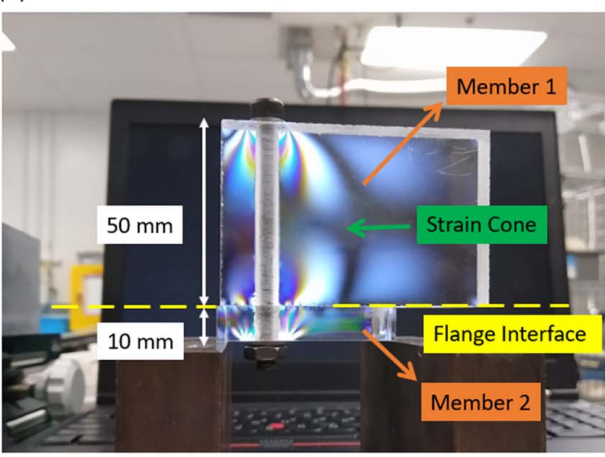


Fig. 5 Photoelastic experiments for stress field observation: (a) stress field observation with 10 mm and 3 mm thick plates and (b) stress field observation with 50 mm and 10 mm thick plates

011027-4 / Vol. 1, 2022 Transactions of the ASME

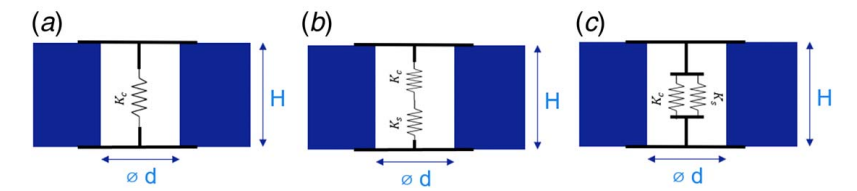


Fig. 6 Different stiffness models: Understanding the role of shear stiffness in a bolted connection: (a) Model 1: compression stiffness only, (b) Model 2: compression with shear stiffness parallel, and (c) Model 3: compression with shear stiffness series

The stiffness value of the member plate could be successfully accounted for by the compression stiffness model without the need for shear stiffness contribution from the member plate. This makes logical sense because for the shear stiffness to play a role, there should be a constraint parallel to the direction in which force is applied. Without a shear constraint, the plate experiences no resistance other than that governed by the compression of the member.

Relationship between member shear stiffness and external constraints

a. Analytical and FEA models

For cases where external constraints are added to the member plates clamped by a bolted connection, a simple bolted connection spring model, which just takes compression stiffness into account, does not appear to be sufficient. An external fixed constraint on one of the bolted members contributes a shear stiffness component to the bolted connection. To understand this better, three different spring models for Maruyama's member stiffness experiment were hypothesized as shown in Fig. 6. Model 1 accounted for stiffness due to compression of the members only. Model 2 accounted the both member compression and shear stiffness connected in parallel while Model 3 considered both the member shear and compression stiffness to be connected in series. The results from analytical models were compared to two FEA cases as represented in Fig. 7. In the first case, no constraints were placed on the nodes surrounding the bolt head area while in the second case, constraints were present on the surrounding nodes. The stiffnesses for all these five cases were plotted as a function of H/d, where H was the thickness of the plate and d was the bore diameter. The results were shown in Fig. 8.

b. Calculation of member shear stiffness

The analysis to determine the member compression stiffness was outlined via Eqs. (1)–(10). Therefore, this section outlines the equations to calculate member shear stiffness. Slocum [13] derives a formula for calculating the shear stiffness of a bolted member given by Eq. (11).

$$C_{\text{bed|shear}} = \frac{\log_e 2}{2\pi t G} \tag{11}$$

where, G is the shear stiffness of the flange member, and t is the thickness. The thickness "t" in Eq. (11) is really the effective thickness of the bolted member which is experiencing shear strain. From Eq. (11), one might argue that as the thickness of the bolted member keeps increasing, the shear stiffness should keep increasing. However, after a point, the shear stiffness of the bolted member saturates because the additional thickness outside the region of influence does not contribute to shear stiffness. A shear strain analysis plot for the member stiffness experiment conducted by Maruyama [16] shows that the region of influence of the preload force extends only up to a limited number of elemental layers.

c. Results and observations

• In cases where external surrounding constraints are applied on the bolted members, Model 2 which considers the member

- compression and shear stiffness in parallel seems to be in reasonable agreement with FEA prediction and hence, is the most appropriate one to use.
- When no external surrounding constraints are applied to the bolted members and they are free to deform under the action of preload force, Model 1 which considers only the compression stiffness seems to be in reasonable agreement with FEA prediction and hence, is the most appropriate one to use.
- The disagreement between the analytical models and FEA curves increases significantly for *H/d* ratios less than one. It can be seen that as *H/d* ratios < 1, Model 1 no longer corresponds to the FEA results. The member compression stiffness formulas predict overly large values compared to FE. Since Models 2 and 3 also use the same member compression stiffness formulas, the effect is reflected in those models as well. As the *H/d* ratio decreases, the member plate essentially transitions from a "thick" plate to a "thin" plate. It seems that the member compression stiffness formulas break down in case of plates that are thin relative to the bolt diameter. It is interesting to note that the breakdown starts at around the golden ratio of 1.6.
- Predictions from Model 3 (with shear and compressive stiffness in series) do not correspond to FEA results.
- The overall axial member stiffness tends to decrease initially as the *H/d* ratio increases but then saturates after a point.

d. Conclusions

The role of shear stiffness in the spring model of a bolted connection depends on the state of external constraints imposed on the bolted members. If the material surrounding a particular bolted member is fixed, there will be a shear stiffness component added to the joint spring model due to that constraint.

For the case of the bolted bearing support structure (i.e., a pillow block), since fixed constraints are applied on the material surrounding the bolted connection, a shear stiffness contribution from the bed can be expected. The overall member stiffness for this case can be therefore calculated via Eq. (12).

$$K_{\text{member}} = \frac{1}{C_{\text{flange}|\text{comp}} + \left[\frac{1}{C_{\text{bed}|\text{comp}}} + \frac{1}{C_{\text{bed}|\text{shear}}}\right]^{-1}}$$
(12)

b. Bolt stiffness calculation:

As per Shigley [11], the bolt stiffness is given by Eq. (13). Conservatively, the area of the threaded portion (A_t) of the bolt is based on the root diameter. Table 8-2 from Shigley [11] gives a higher order estimate of A_t based on the average of the pitch and root diameters. For 1/4-20 UNC bolt, A_t was 0.0318 in.² or 20.52 mm².

$$K_{\text{bolt}} = \frac{A_d A_t E}{A_d l_t + A_t l_d} \tag{13}$$

$$A_d = \frac{\pi d^2}{4} \tag{14}$$

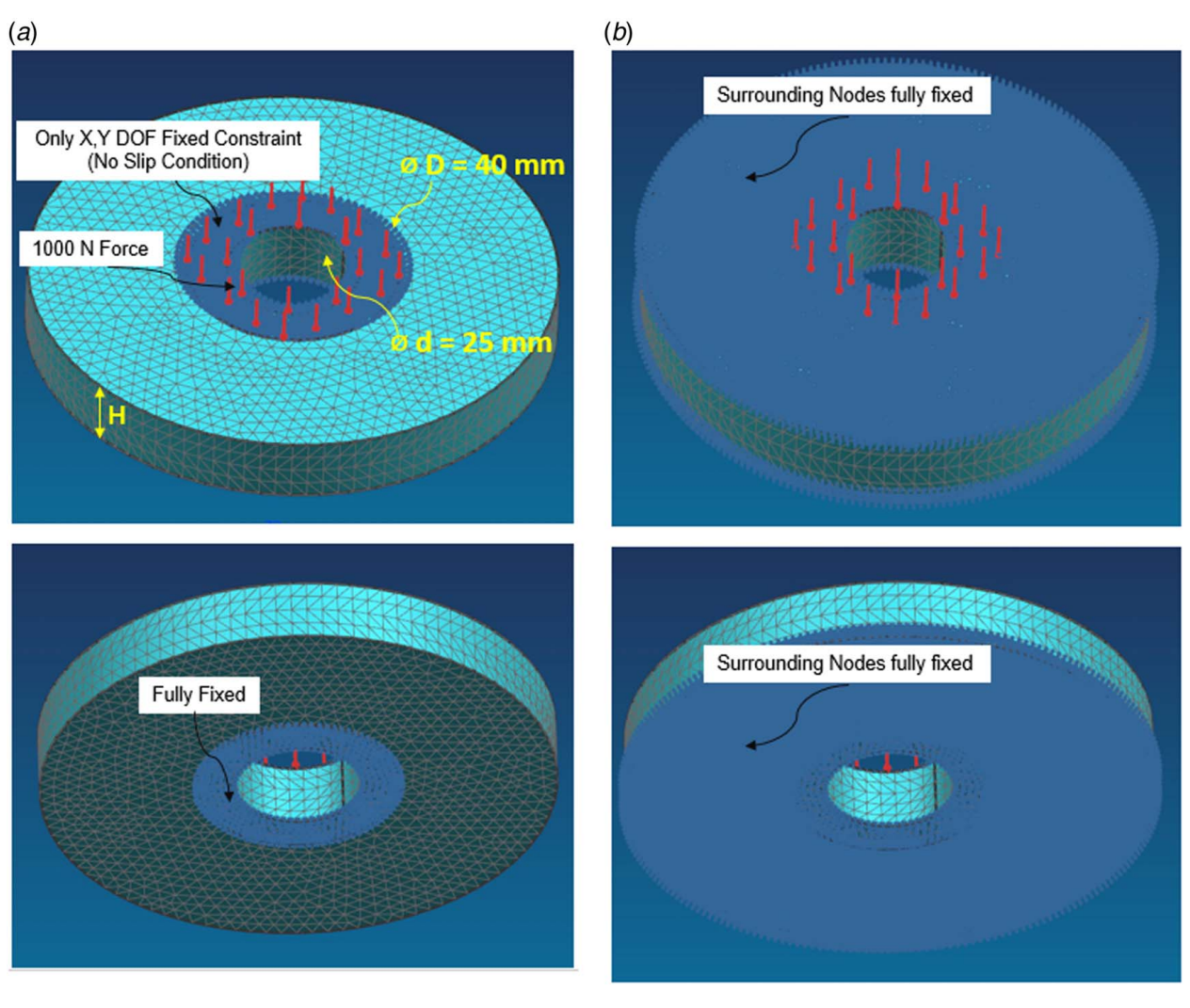


Fig. 7 Constrained and unconstrained FEA models used for shear stiffness investigation: (a) FEA model with no constraints on surrounding nodes and (b) FEA model with fixed constraints on surrounding nodes

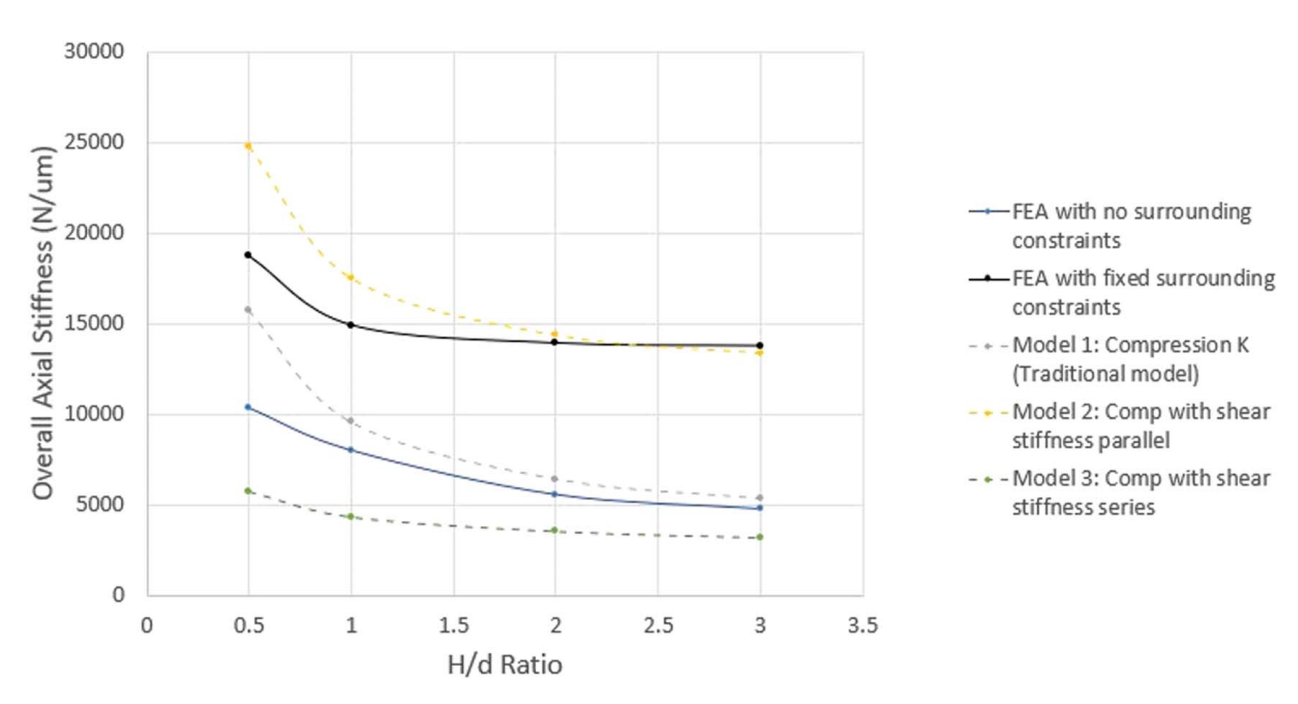


Fig. 8 Stiffness as a function of cone parameters

011027-6 / Vol. 1, 2022 Transactions of the ASME

c. Total axial stiffness calculation:

The bolt provides preload to the joint and its stiffness will be in parallel to the stiffness of the material it compresses. Therefore, the axial stiffness of the joint is given by Eq. (15).

$$K_{\text{axialioint}} = K_{\text{member}} + K_{\text{bolt}}$$
 (15)

2.4.2 Pitch Stiffness Calculation. Next, a relation between the axial joint stiffness and the pitch stiffness needs to be established. The pressure distribution profile at the joint interface is shown in Fig. 9. A model presented by Slocum [13] for roller bearings is used here for the bolted joint and it assumes a similar pressure distribution profile to develop a differential stiffness expression and derive an equation relating the axial stiffness of the bolted joint to the pitch moment stiffness.

a. Derivation of relation between axial stiffness and pitch stiffness;

Consider an infinitesimal element (dx) of the pressure profile shown in Fig. 9. Since the pressure profile is linear, the pressure value of this element located at a distance x from the center of the width of the pillow block can be found by multiplying the slope of the line with the distance from the center of the pillow block width. The resulting force that this infinitesimal element exerts on the base is given by Eq. (16).

$$dF = \frac{P_{\text{ext}}}{W/2} Lx dx \tag{16}$$

The moment equation can be written as per Eq. (17).

$$dM = 2*\frac{P_{\text{ext}}}{W/2}Lx^2dx \tag{17}$$

Integrating to calculate the total moment,

$$M = \frac{4P_{ext}L}{W} \int_{0}^{W/2} x^{2} dx$$
 (18)

$$M = \frac{4P_{\text{ext}}L}{W} \left[\frac{x^3}{3} \right]_0^{W/2} = \frac{P_{\text{ext}}LW^2}{6}$$
 (19)

Assuming that a pressure $P_{\rm ext}$ acting on a contact area of width W and length L causes a deflection δ , the linear stiffness $(K_{\rm linear})$ can be given by

$$K_{\text{linear}} = \frac{P_{\text{ext}}LW}{\delta} \tag{20}$$

As shown in Fig. 10, using the small-angle approximation, $\delta = \theta * W/2$. Substituting Eq. (20) in Eq. (19),

$$M = \frac{K_{\text{linear}}\delta W}{6} \tag{21}$$

The pitch stiffness is thus realized as follows:

$$K_{\text{pitch}} = \frac{M}{\theta} = \frac{\frac{K_{\text{linear}}\delta W}{6}}{\frac{\delta}{W/2}} = \frac{K_{\text{linear}}W^2}{12}$$
 (22)

Here, the assumed pressure profile is symmetric and acts across the whole width. Also, the K_{linear} , in this case, is equal to $K_{\text{axialjoint}}$.

b. Transformation of pitch stiffness to linear stiffness along the pillow block axis:

Equation (22) suggests that for pitch stiffness of the bolted connection, the width of the member on which the moment is being applied and the axial stiffness of the bolted connection play a major role.

Assuming, H to be the total height of the pillow block and H_c to be the height of the pillow block axis from the fixed base, the equivalent stiffness of the structure in the direction of the force can be calculated by Eq. (23).

$$K_{\text{pitch(along the direction of force)}} = \frac{K_{\text{pitch}}}{H_c H} = \frac{K_{\text{linear}} W^2}{12H_c H}$$
 (23)

2.5 Total Stiffness Along the Pillow Block Axis. As shown in Fig. 2, all the four calculated stiffness values are in series. Therefore, the total axial stiffness of the pillow block can be written as follows:

$$\frac{1}{K_{\text{total}|\text{axial}}} = \frac{1}{K_{\text{housing}|\text{bending}}} + \frac{1}{K_{\text{housing}|\text{shear}}} + \frac{1}{K_{\text{housing}|\text{torsional}}} + \frac{1}{K_{\text{pitch(along the direction of force)}}}$$
(24)

For the derivation of the pillow block body stiffness (including housing bending, shear and torsional stiffnesses), please see Supplemental Material on the ASME Digital Collection.

3 Experimental Setup

Figure 11 shows an overview of the experimental setup. A pillow block made of plain carbon steel was bolted onto an aluminum base. The preload on the bolt was set to the desired level. For a maximum force of 360 N along the pillow block axis, the required bolt preload was calculated to be 1350 N, which corresponded to a torque requirement of about 5.68 Nm. Detailed calculations for critical loads to prevent loss of preload and gross slip can be seen in the Supplemental Material on the ASME Digital Collection. An aramid rope is used to pull so that no moment is applied on the pillow block. A linear variable differential transformer (LVDT) sensor with 100 nm least count is used to measure the deflection of the tip of the pillow block.

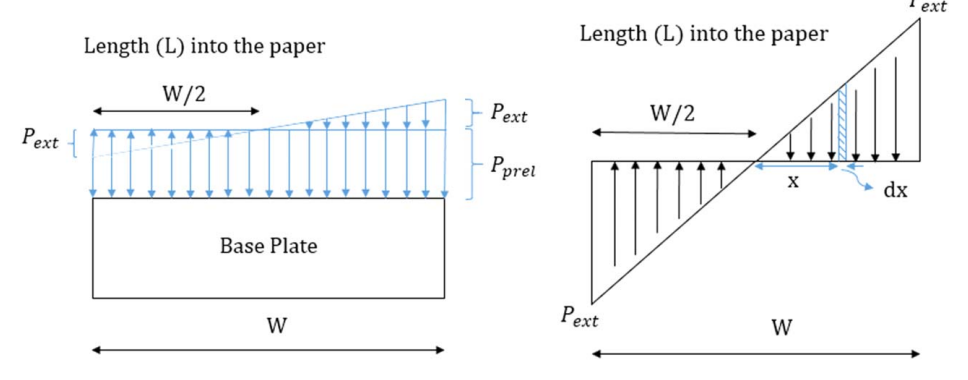


Fig. 9 Derivation of relation between linear and pitch stiffnesses

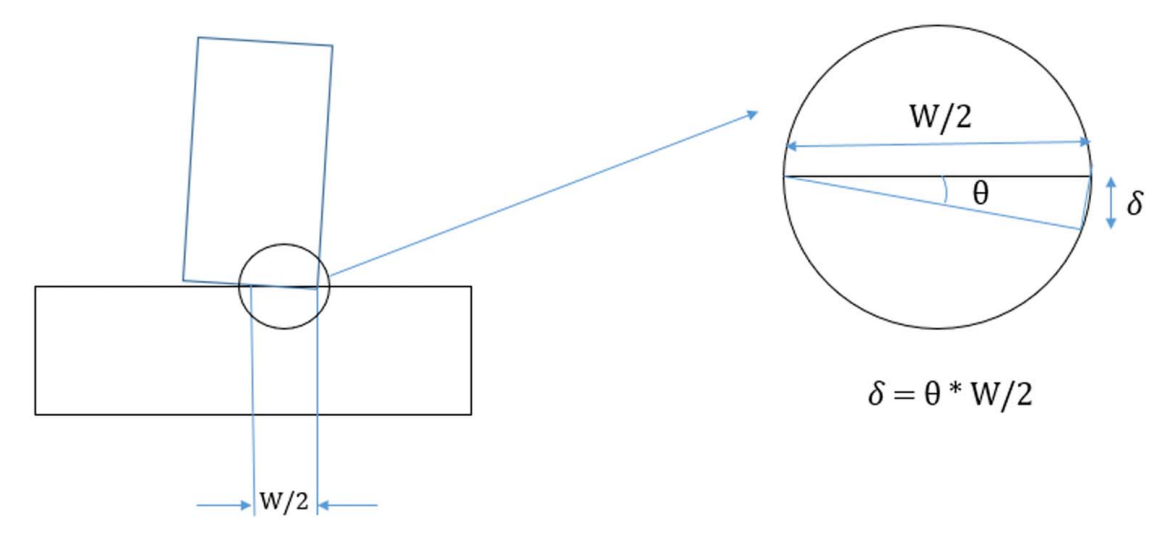


Fig. 10 Relation between angular and linear deflections

A digital spring scale was used to measure the applied force. The pillow block assembly was held in place on the granite block using two C clamps. The LVDT sensor was mounted on the base plate itself via a magnetic base indicator holder and the magnetic base was attached to the test assembly via an intermediate plate of low-carbon steel. This was done to avoid parasitic errors associated with the deflection of the base plate itself with respect to the granite surface. The deflection of the pillow block was to be measured at its top in the direction of application of force.

4 Finite Element Analysis Studies

FEA studies were conducted using NX 11 advanced simulation software which is based on NASTRAN. Throughout the literature, many different FEA models have been used to simulate bolted connections. Some of these models are no-bolt, coupled bolt, spider bolt, and solid bolt. While the solid bolt model appears to be the best simulation approach for accuracy, it requires extra computation effort and use of contact elements at interfaces [17]. The spider bolt model, on the other hand, is much more computationally efficient

with reasonable accuracy close to the solid bolt model. The spider bolt model represents the bolt head/nut and shank with line elements. The bolt shank can be modeled using a CBAR line element, which is essentially a simplified circular beam element with stiffness governed via the cross section area and material properties defined by the user. The line elements representing the bolt head/nut are modeled using RBE3 elements. RBE3 are rigid body elements generally used in finite element analysis for load transfer. Both CBAR and RBE3 elements are standard elements in the FEA library. The line elements representing the bolt head/nut look like a spider web connected to mesh structure of the flange members, hence named as spider bolt model. In this FEA study, the bolted connections are represented using the spider bolt model.

4.1 Finite Element Analysis Model Setup

4.1.1 Meshing and Finite Element Method Model Creation. Various element types were used to model the components of the bolted pillow block system. CTETRA(10), a quadratic 3D solid element, was used to model the base and the pillow blocks.

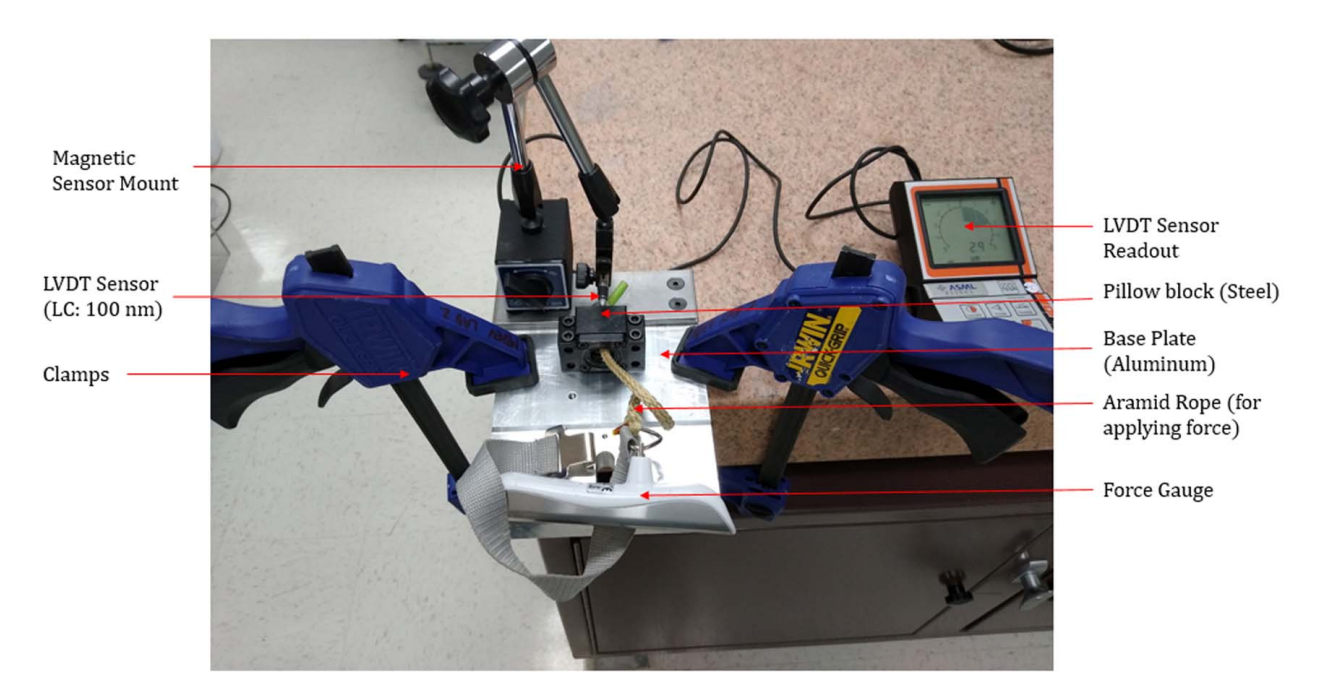


Fig. 11 Experimental setup

011027-8 / Vol. 1, 2022 Transactions of the ASME

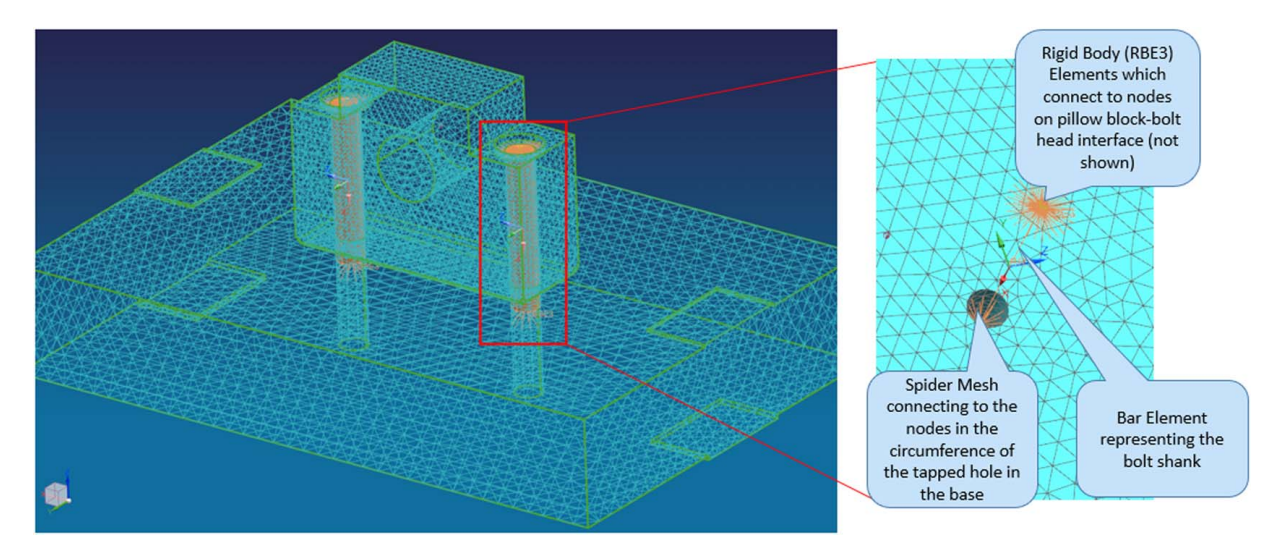


Fig. 12 Spider bolt model: Mesh construction details

CBAR element was used to model the bolt shank whereas RBE3 elements were used for the spider connection. An element quality check of the mesh indicated no failed elements.

Figure 12 shows the spider mesh used to create the bolted connection. In a spider bolt model, the head and the nut (or threaded hole) are modeled as rigid body elements connected to the clamped members. The bolt shank is represented as a bar element (with the same cross section area). The spider mesh in the base plate tapped hole extends upto a depth equal to the thread engagement of the bolt (equal to approximately 1.3 bolt diameters). The other end of the spider mesh connects to surface nodes on the pillow block at the bolt head interface. The radial extent to which these connections are to be made is defined based on the diameter of the bolt head.

4.1.2 Application of Loads and Constraints. Figure 13 shows an overview of the loads and constraints applied in a general bolted connection model. The Y-direction force is applied along the inner circumference of the pillow block bore and bolt preload force is applied on each bolt. The bolt preload was represented in the FEA model using the bolt preload feature in NX Advanced Simulation. This feature helps engineers apply bolt preload forces. To achieve bolt-pretension, the FEA software essentially cuts the meshed body into two and uses pretension elements to write a constraint equation that relates the displacement of the cut boundaries accordingly [18]. In the FEA model and the experiment, the base plate was fixed at the side tabs as indicated in Fig. 13. There are four such regions in total (two on the top and two on the bottom). The interface area of the tabs was same as that of the

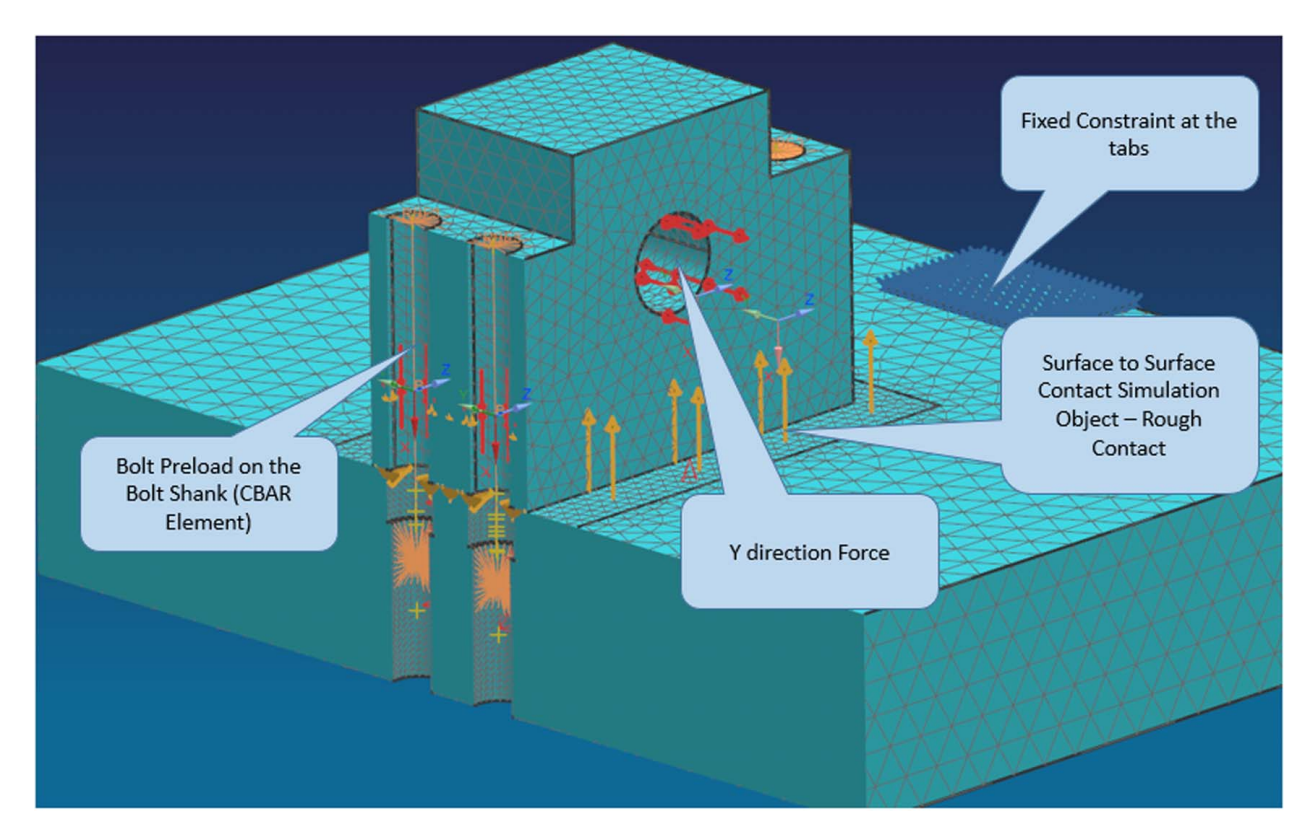


Fig. 13 Spider bolt model: Loads and constraints

Table 2 Final results summary (comparison of analytical, FEA, and experimental results for all three pillow blocks)

		pillow block along pplied transverse lo		Error of the	ne analytical model
Pillow blocks	Analytical	FEA	Experimental	w.r.t FEA	w.r.t Experimental
2-bolt steel 4-bolt steel 2-bolt PLA	70.8 N/um 133.6 N/um 5.6 N/um	75 N/um 126.6 N/um 7.4 N/um	60 N/um 113 N/um 6.6 N/um	-5.6% 5.5% -24.3%	18% 18.2% -15.1%

clamps used in the experimental testing. A surface-to-surface contact simulation object was added to the model. This simulation object creates contact elements at the pillow block-base plate interface. Contact modeling requires the definition of a pair of surfaces called the source and the target. If the mesh size for both the surfaces is different, it is recommended that the surface with smaller mesh size, be the source. This is because contact check is always performed from the source side towards the target side. Normal projections are extended from the nodes on the source surface to the target surface. Hence, if the source surface has smaller mesh size, the contact check can be performed with greater accuracy. No slipping was allowed in the model. Preload for each of the bolts was set to 1350 N.

5 Verification of the Analytical Model Via Finite Element Analysis and Experiments

A summary of the analytical, FEA, and experimental results for all three pillow block cases is shown in Table 2. The analytical model is in reasonable agreement with the FEA predictions and experimental data. For detailed results and discussions on each pillow block case, please see Supplemental Material on the ASME Digital Collection.

6 Case Studies on Application of the Analytical Model

To demonstrate the use of the analytical model for moment stiffness of bolted connections, two case studies are presented that focus on ball screw bearing support structures (i.e., pillow blocks):

- a. Machine tool linear axis—This case study highlights the selection of an appropriate bearing support block based on stiffness matching with other components in ball screw drive (screw, nut, and bearings) to meet the desired performance requirements for a machine tool linear axis.
- b. High-speed 3D printer—This case study highlights the selection of a ball screw support for a high-speed 3D printer.

The stiffness contribution from ball screw drive components is typically assumed from catalog values for nut stiffness, if even available, or ignored in conventional models, and just shaft stiffness is considered as the dominant compliance. Various research studies have proposed better alternative stiffness models by closely accounting for such contributions from components/aspects ignored in the conventional models. For example, Okwudire [19] proposed an improved screw-nut interface model by considering the effect of elastic deformation of the screw portion inside the nut. This model enabled a better prediction of the natural frequencies of the ball screw drive system. Similarly, bearing support blocks are an essential component in the structural loop whose stiffness contribution has typically been ignored in conventional models or at best is assumed to be equal to the nut stiffness. Since bearing blocks are generally bolted onto the machine frame, the analytical model for moment stiffness of bolted connections proposed in this paper can be applied to a ball screw bearing support block to account for its effect on the drive system stiffness and dynamics.

6.1 Machine Tool Linear Axis

6.1.1 Introduction. Machine tool axes are subject to very high forces and thus require high stiffness actuators which are most often ball screws. Guidelines and formulas are available to predict the stiffness of the screw shaft, nut, and support bearings, but analytical models are needed to estimate the bearing housing stiffness which is usually bolted on a stiff mounting base. Often there is an offset between the line of action of ball screw thrust force and the interface between the bearing block and the base to which it is bolted. This results in a moment load being applied on the bolted bearing block which in turn contributes to a load induced axial positioning error in the system. Contact stiffnesses at the various joint interfaces of a machine tool also play a vital role in determining its dynamic performance [20].

6.1.2 Selection of Stiffness Matched Bearing Blocks. A spreadsheet, presented in Supplemental Material on the ASME Digital Collection, has been created to aid the designer in selecting the appropriate bearing block housing based on the stiffness values of other ball screw drive system components. A calculation flowchart is shown in Fig. 14. First, the operating parameters of the ball screw drive system like the move profile, travel distance, carriage mass, process force, etc., are entered. An initial "guesstimate" is made for the screw shaft diameter, length, and material which determines the screw shaft stiffness. The next step is to then to initially specify the screw lead, nut, and support bearings. Generally, the screw lead is chosen such that the inertia ratio is close to one for optimal power transmission. The spreadsheet then calculates the minimum required bearing block stiffness.

A plot of total system stiffness and the bearing block stiffness is automatically updated in the spreadsheet according to the parameters entered. After finding the minimum recommended stiffness values for the bearing blocks, the designer then enters information regarding the bearing block geometry, mounting base, and the bolts used to secure the bearing block. The spreadsheet calculates the actual bearing block stiffness based and tries to find the closest matching bearing block from a pre-existing catalog of various bearing blocks (e.g., from McMaster-Carr [21]). The designers also have the capability to expand this catalog according to their needs.

Designers can also refer to Fig. 15 which shows a 3D design plot of the recommended bearing block stiffness as a function of the length and diameter of the selected ball screw shaft. Using this plot, the designer can choose the best combination of the screw shaft, screw diameter, and bearing block stiffness while meeting a particular system stiffness requirement. This plot was generated for reference only by using reasonable estimates for the stiffness of the nut and the support bearings. A design engineer could adjust stiffnesses accordingly for the intended application.

6.1.3 Representative Bearing Blocks. Representative bearing blocks (McMaster-Carr catalog [21]) were considered where the two parameters most significantly affecting the pitch stiffness of bearing blocks are the diameter of bolts used to secure the bearing block to the base and the ratio of the width of the block (W) to its center height (Hc). Figure 16 plots the bearing block stiffness as a function of the bolt diameter and the bearing block

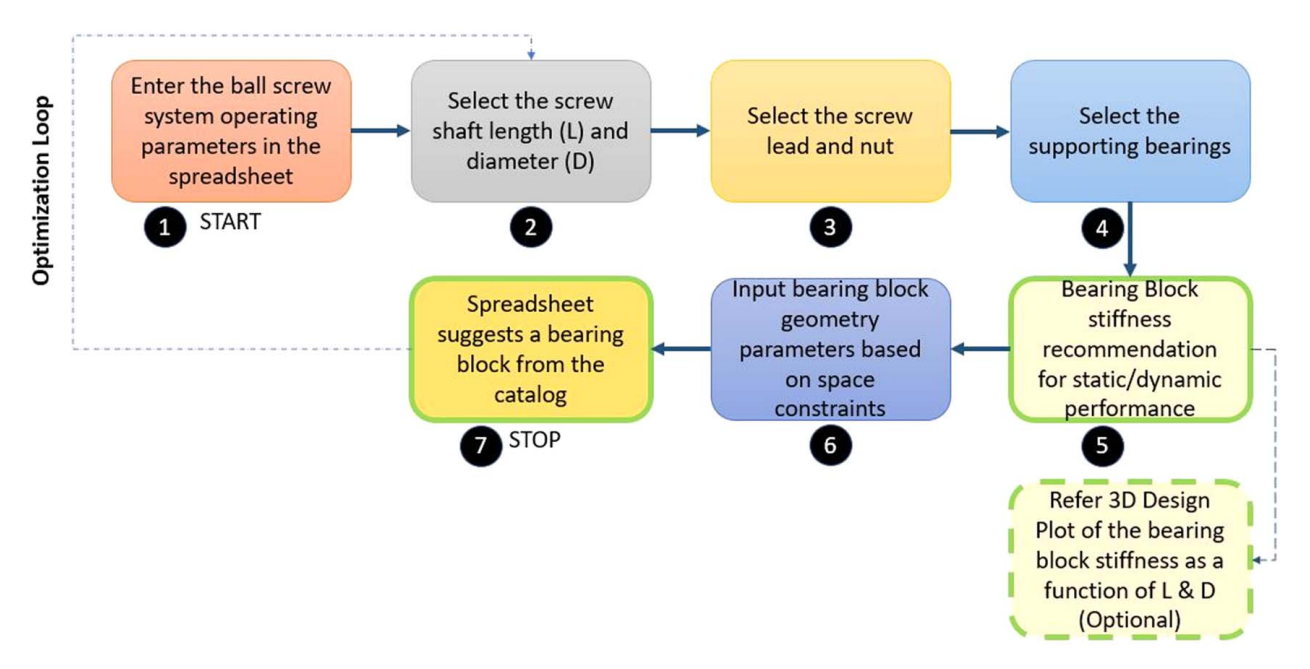


Fig. 14 Ball screw analysis spreadsheet—calculation flowchart

geometry parameters (*W/Hc* ratio). The light coloured circles represent 4-bolt bearing blocks and the blue circles represent 2-bolt bearing blocks. The size of the circles corresponds to the cost of the bearing blocks. The numerical values next to the circles represent the stiffness of the bearing blocks in N/um.

Is it better to have a 4-bolt bearing block with smaller bolt diameter or a 2-bolt bearing block with bigger bolt diameter? Or what is the cost to stiffness trade-off between various types of bearing blocks? Fig. 16 seeks to answer such questions and serve as a reference tool for designers to balance the cost and stiffness trade-off among various bearing block options. Although the stiffness values are calculated assuming that the bearing blocks will be mounted on an aluminum base using steel bolts, the user can update these numbers in the spreadsheet to generate a trade-off plot representing their application more accurately. One of the key observations from this graph is that there are generally four

different groups of pillow blocks. Table 3 details the cost and stiffness ranges for these four groups. Group 1 represents the highest stiffness pillow blocks which use big diameter bolts and have a high *W/Hc* ratio. Groups 2 and 3 are medium stiffness pillow blocks that either have a high *W/Hc* ratio or a use bigger diameter bolt. Group 4 is low stiffness pillow blocks, which has both low *W/Hc* ratio and smaller bolt diameters. Although Group 4 bearing blocks have low stiffness, they offer a compact footprint for systems which have volume limitations.

6.2 High-Speed 3D Printer. The objective of this case study is to describe how to select an appropriate ball screw support for a high-speed 3D printer. 3D printers are generally not subjected to large external loads, but this can lead to a false sense of security, and some end up being undersized for the dynamic performance

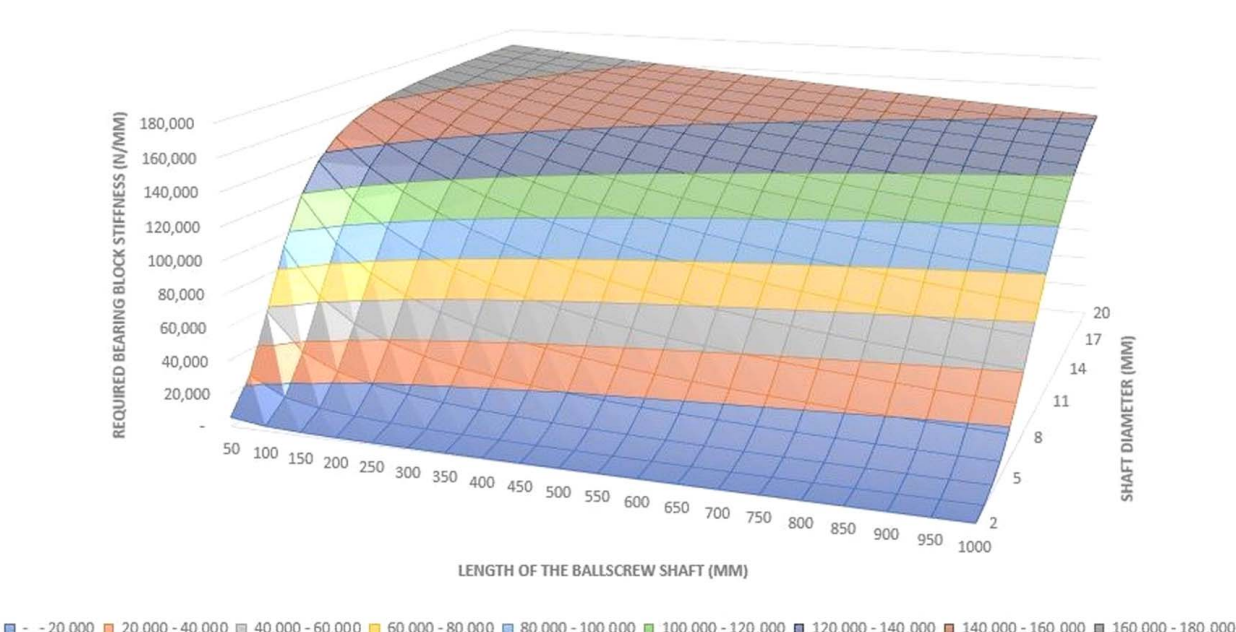


Fig. 15 Required bearing block stiffness as a function of ball screw shaft length and diameter

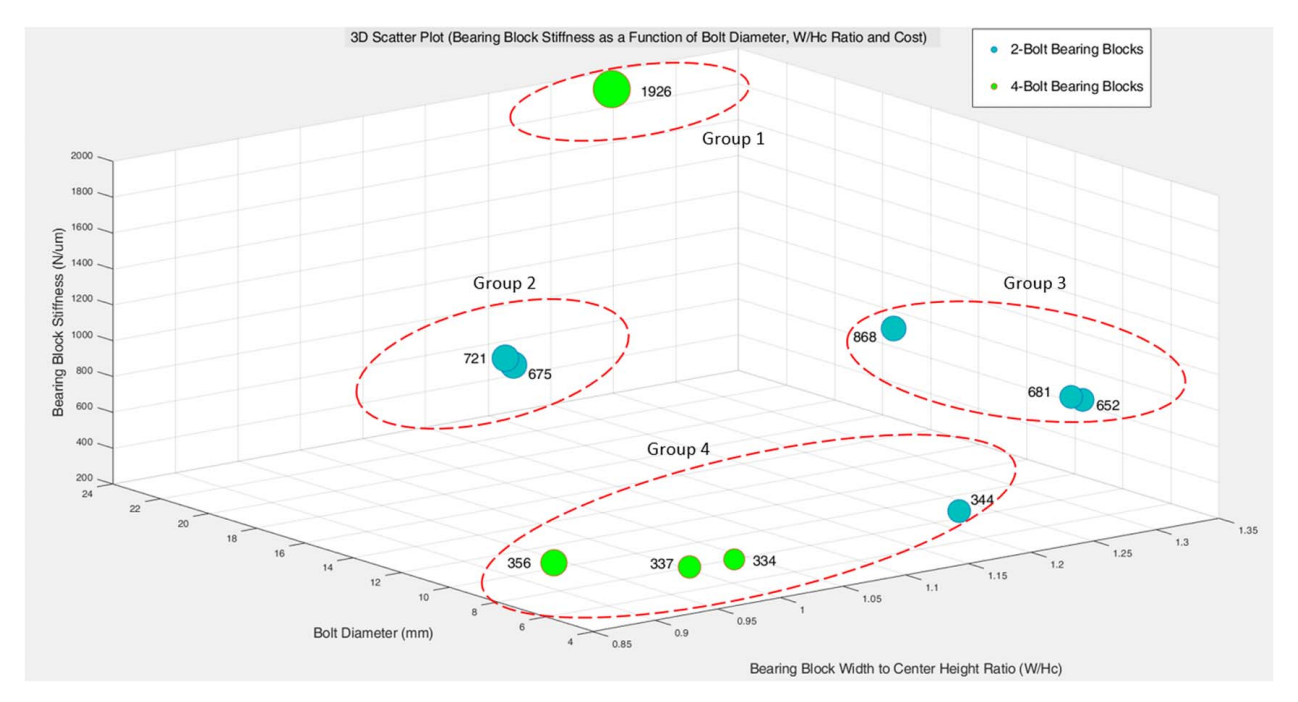


Fig. 16 3D scatter plot of bearing block stiffness as a function of bolt diameter, W/Hc ratio, and cost

Table 3	Cost versus stiffness com	parison of various bear	na block types	(mounting base	material: aluminu	ım)

Group #	W/Hc ratio	Bolt diameter (mm)	Stiffness range (N/um)	Cost range (USD)
1	High (1.2–1.4)	High (15–25)	High (~2000 or more)	~1400 or greater
2	Low (1-1.2)	High (15–25)	Medium (600–750)	~600–700
3	High (1.2–1.4)	Low (6–15)	Medium (600–900)	~500–650
4	Low (1-1.2)	Low (6–15)	Low (300-400)	~400–700

required. Ball screw assembly dynamics can significantly limit the throughput.

While a smaller diameter ball screw reduces system inertia leading to faster response times, it also reduces the screw shaft stiffness leading to lower natural frequencies. Axial vibrations are just one of the many modes of vibration that the ball screw shaft is susceptible to. High lead/diameter ratio screws also suffer from torsional windup that must be considered as part of the effective axial stiffness of the screw (Slocum [13]) Due to the coupling introduced by the nut, the application of torque on the ball screw can also cause unwanted lateral vibrations of the ball screw, thereby affecting the system's positioning accuracy. Okwudire [22], in fact, showed analytically that while the torque induced lateral vibrations cannot be completely eliminated, but they can be reduced by wisely choosing the entry/exit angles of the balls in the ball screw drive mechanism. Slocum [13] discusses many of the factors affecting well-known optimal transmission ratio formulas for two categories of systems: ones which encounter large external forces during operation and others for which the encountered external forces are negligible. Since 3D printers fall in the latter category, the simple inertia dominated formula may be used to determine the optimal transmission ratio (n) as shown in Eq. (25).

Optimal|Transmission|Ratio|(n) =
$$\sqrt{\frac{J_{\text{load}}}{J_{\text{motor}}}}$$
 (25)

For a direct drive connection between the motor and shaft (transmission ratio = 1), optimal power transmission is achieved when the inertia of the motor is equal the inertia of the driven load, but when satisfying the inertia ratio, the shaft diameter, and hence axial

stiffness, may be limited thereby placing greater stiffness requirements on the bearing support block. In addition, high lead/diameter ratio screws are often selected which can lead to effective axial stiffness decrease due to torsional windup of the shaft as derived by Slocum [13].

The throughput of a 3D printer can be assumed to scale along the lines of the maximum achievable angular velocity of the ball screw shaft. Similarly, one of the contributors to the cost of a 3D printer is the servomotor/amplifier package which generally scales with the power rating of the motor.

6.2.1 Throughput Dependency on the Bearing Block Stiffness. Suppose a designer's objective is to maximize the throughput of the 3D printer while keeping the same motor power and system natural frequency. Since the ball screw shaft and the bearing block act as springs connected in series with one another, the designer can try to minimize the ball screw shaft diameter and maximize the bearing block stiffness to maintain the same system natural frequency. Reducing the diameter of the ball screw shaft reduces the rotary inertia of the system which in turn leads to a higher achievable angular acceleration. Figure 17(a) shows how the maximum achievable angular velocity increases as a function of the bearing block stiffness. Quite predictably, the benefit of using a stiffer bearing block wanes after a certain point. While stiffening the bearing block helps limit impact to the natural frequency for the axial vibration mode, the natural frequencies for other vibration modes (e.g., torsional and lateral modes) may still be impacted significantly with reduction in shaft diameter.

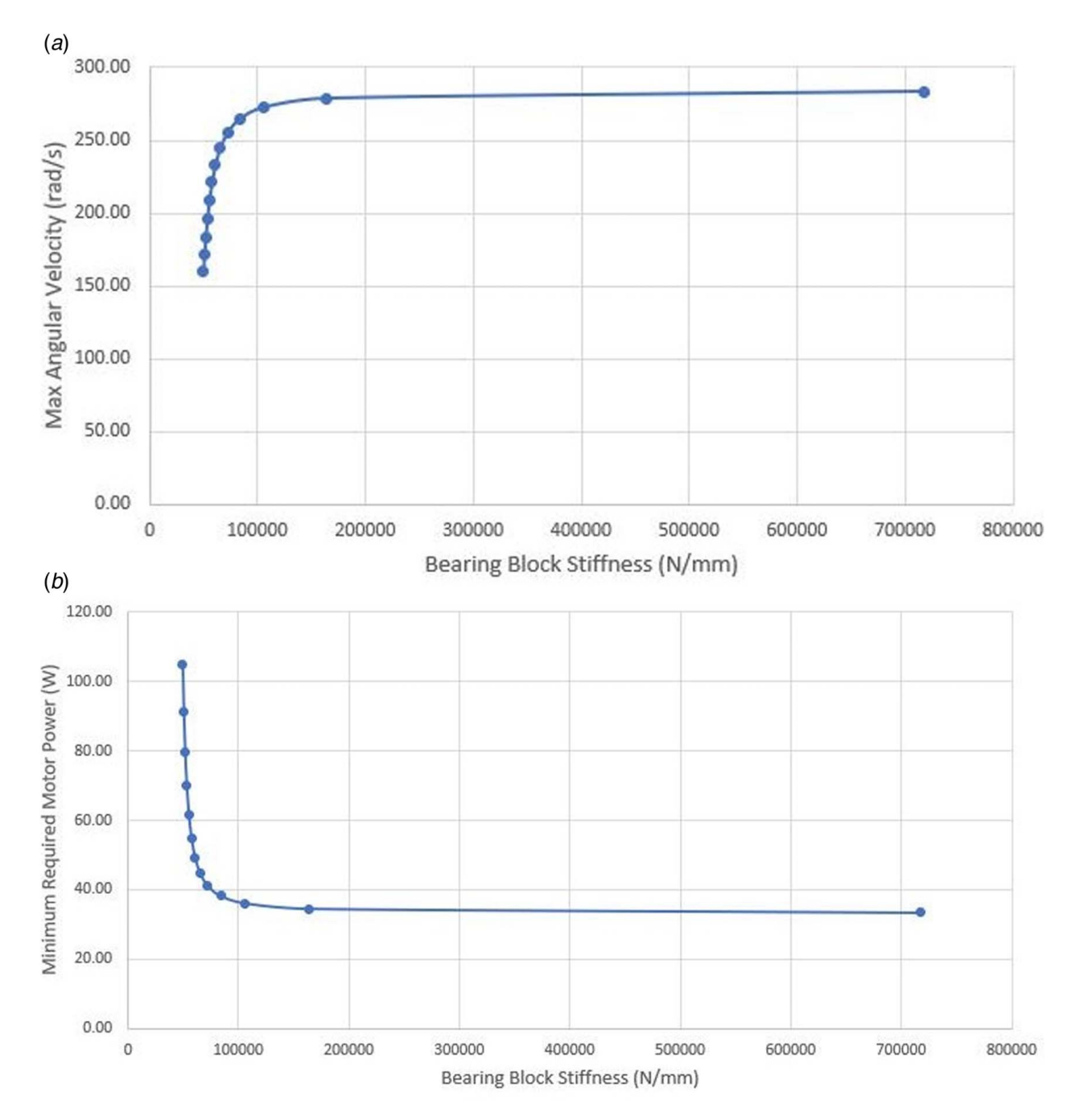


Fig. 17 Throughput and cost dependency on bearing block stiffness: (a) maximum angular velocity as a function of bearing block stiffness and (b) minimum required motor power as a function of bearing block stiffness

6.2.2 Cost Dependency on the Bearing Block Stiffness. Using a stiffer bearing block with a smaller diameter ball screw shaft may also be a good strategy to reduce the cost of a 3D printer without impacting its throughput. If the same strategy of minimizing the rotary inertia of the system while maintaining the system natural frequency is followed, the designer will need a motor with lower power rating to achieve the same angular velocity of the shaft. Reducing motor size or power reduces the cost of the servomotor and amplifier package accordingly [13]. Figure 17(b) shows the required motor power as a function of the bearing block stiffness. It can be seen that the minimum required motor power falls drastically at first as the bearing block stiffness is increased but then the curve saturates very quickly. Based on Fig. 17(b), an optimal choice for a bearing support block in this case will be one with a stiffness of at least 100 N/um. Irrespective of the type of bearing block the

designer uses, there is a minimum limit to the required motor power based on the required move profile and other operating parameters.

7 Conclusions

An analytical model for predicting the pitch stiffness of bolted connections has been presented. This model is verified by finite element analysis and experimental testing. Three different pillow blocks were used as test cases for this verification. For all three cases, the load deflection curves for analytical, experimental, and FEA results are in reasonable agreement. Observations from these studies include as follows:

- Beware subtle sources of compliance in the experimental setup.
- Micro slip may occur at the pillow block-base plate interface.
 To make sure that the measurements can be attributed to elastic system stiffness, one should check that there is no residual deflection once the system is unloaded.
- It is important to choose test cases where the dominant source of compliance is the focus of the study. It is very difficult to isolate individual sources of compliance during experimental testing.
- For a multi-bolt pattern, it is important to follow the recommended tightening sequence (according to whether the pattern is circular or non-circular). At least two tightening cycles should be used across the bolt pattern to minimize variation in preload due to bolt cross-talk.
- It is important to be aware of geometrical limitations of the object of interest (e.g., pillow block in this case). The strain cone field saturates prematurely if the bolts are too close to the edges of the pillow block. In such cases, one should try estimating the stiffness of the flange members as per their geometrical limitations.
- In an FEA study, close attention should be paid to the finite element mesh. Refining the mesh at the important interfaces and verifying mesh convergence are important steps to get accurate and trust-worthy results.
- Close attention should be paid to the external constraints applied on the bolted joint system and how it affects the overall joint stiffness model. Section 2.4.1 detailed how the contribution of the member shear stiffness to the overall bolted joint stiffness depends on the state of the external constraints imposed on the members.
- The application of the presented analytical model for selection of ball screw bearing support blocks has been illustrated via two case studies: one is based on a machine tool linear axis and another is based on a high-speed 3D printer. The capability of predicting the stiffness of bearing support blocks may help designers to optimize a ball screw system as per their system requirements, whether it be maximizing system throughput, reducing cost, improving the system's natural frequency, or reducing load induced positioning errors.

The analytical models developed in this paper can be readily incorporated into a design spreadsheet, as part of a product's design history file, for rapidly considering "what-if" scenarios. Later, once a workable design has been developed, it can be fine-tuned with a more elaborate finite element model.

Acknowledgment

The authors would like to thank John Massucci, Geoffrey Williams, and Phil LaMastra from ASML US LP for providing access to the computational resources and FEA software (NX Advanced Simulation 11) used in this study. The authors would also like to thank John Fortunato, Jim Chester, Andy Hamilton, and Dragos Pariza from ASML US LP for their valuable advice and suggestions. This research did not receive any specific grant from funding agencies in the public, commercial, or not-for-profit sectors.

Conflict of Interest

There are no conflicts of interest. This article does not include research in which human participants were involved. Informed consent is not applicable. This article does not include any research in which animal participants were involved.

Data Availability Statement

The datasets generated and supporting the findings of this article are obtainable from the corresponding author upon reasonable request.

References

- Zhang, O., and Poirier, J. A., 2004, "New Analytical Model of Bolted Joints," ASME J. Mech. Des., 126(4), pp. 721–728.
- [2] Nassar, S. A., and Abboud, A., 2009, "An Improved Stiffness Model for Bolted Joints," ASME J. Mech. Des., 131(12), p. 121001.
- [3] Wileman, J., Choudhury, M., and Green, I., 1991, "Computation of Member Stiffness in Bolted Connections," ASME I. Mech. Des. 113(4) pp. 432–437
- Stiffness in Bolted Connections," ASME J. Mech. Des., 113(4), pp. 432–437.
 [4] Lehnhoff, T. F., Ko, K. I., and McKay, M. L., 1994, "Member Stiffness and Contact Pressure Distribution of Bolted Joints," ASME J. Mech. Des., 116(2), pp. 550–557.
- [5] Sethuraman, R., and Sasi Kumar, T., 2009, "Finite Element Based Member Stiffness Evaluation of Axisymmetric Bolted Joints," ASME J. Mech. Des., 131(1), p. 011012.
- [6] Ito, Y., and Masuko, M., 1971, "Study on the Horizontal Bending Stiffness of Bolted Joint," Bull. JSME, 14(74), pp. 876–889.
- [7] Gould, H. H., and Mikic, B. B., 1972, "Areas of Contact and Pressure Distribution in Bolted Joints," ASME J. Eng. Ind., 94(3), pp. 864–870.
- [8] Oskouei, R. H., Keikhosravy, M., and Soutis, C., 2009, "Estimating Clamping Pressure Distribution and Stiffness in Aircraft Bolted Joints by Finite-Element Analysis," J. Aerosp. Eng., 223(7), pp. 863–871.
 [9] Naruse, T., and Shibutani, Y., 2012, "Nonlinear Bending Stiffness of Plates
- [9] Naruse, T., and Shibutani, Y., 2012, "Nonlinear Bending Stiffness of Plates Clamped by Bolted Joints Under Bending Moment," J. Solid Mech. Mater. Eng., 6(7), pp. 832–843.
- [10] Precision Machine Components, NSK Ltd., Tokyo, Japan, 2017, pp. B17–B18.
- [11] Budynas, R., and Nisbett, J., Shigley's Mechanical Engineering Design, 9th ed., McGraw Hill.
- [12] Williams, J. G., Anley, R. E., Nash, D. H., and Gray, T. G. F., 2009, "Analysis of Externally Loaded Bolted Joints: Analytical, Computational and Experimental Study," Int. J. Press. Vessel. Pip., 86(7), pp. 420–426.
- [13] Slocum, A. H., 1995, Precision Machine Design, Society of Manufacturing Engineers, Dearborn, MI, pp. 365–393.
- [14] Du, F., Li, B., Zhang, J., Zhu, Q. M., and Hong, J., 2015, "Ultrasonic Measurement of Contact Stiffness and Pressure Distribution on Spindle-Holder Taper Interfaces," Int. J. Mach. Tools Manuf., 97, pp. 18–28.
- [15] Cao, J., and Zhang, Z., 2019, "Finite Element Analysis and Mathematical Characterization of Contact Pressure Distribution in Bolted Joints," J. Mech. Sci. Technol., 33(1), pp. 1–11.
- [16] Maruyama, K., Yoshimoto, I., and Nakano, Y., December 1975, "On Spring Constant of Connected Parts in Bolted Joints," Bull. JSME, 18(126), pp. 1472–
- 1480.
 [17] Montgomery, J., 2002, Methods for Modelling Bolts in Bolted Joints, Seimens
- Westinghouse Power Corporation, Orlando, FL, Technical Report, p. 8. [18] Oatis, D., 2007, "Analyzing Bolt Pretension in the ANSYS Workbench Platform," ANSYS Adv, 1, pp. 28–29.
- [19] Okwudire, C. E., 2011, "Improved Screw-Nut Interface Model for High-Performance Ball Screw Drives," ASME J. Mech. Des., 133(4),
- [20] Chang, Y., Ding, J., He, Z., Shehzad, A., Ding, Y., Lu, H., Zhuang, H., Chen, P., Zhang, Y., Zhang, X., and Chen, Y., "Effect of Joint Interfacial Contact Stiffness on Structural Dynamics of Ultra-Precision Machine Tool," Int. J. Mach. Tools Manuf., 158, p. 103609.
- [21] "End Supports for Lead Screws and Ball Screws," McMaster-Carr, https://www.mcmaster.com/bearing-blocks/end-supports-for-lead-screws-and-ball-screws-4/, Accessed January 5, 2021.
- [22] Okwudire, C. E., 2012, "Reduction of Torque-Induced Bending Vibrations in Ball Screw-Driven Machines Via Optimal Design of the Nut," ASME J. Mech. Des., 134(11), p. 111008.
- [23] Juvinall, R., and Marshek, K., Fundamentals of Machine Component Design, 5th ed., John Wiley and Sons, Inc., Hoboken, NJ, p. 419.
- [24] Ghosh, S., 2011, Typical Coefficient of Friction Values for Common Materials, MechGuru, https://mechguru.com/machine-design/typical-coefficient-of-friction-values-for-common-materials/, Accessed November 15, 2018.